Available online at www.sciencedirect.com
SCIENCE DIRECT®
International Journal of Solids and Structures 43 (2006) 807–827
INTERNATIONAL JOURNAL OF SOLIDS and STRUCTURES
www.elsevier.com/locate/ijsolstr

Subcritical crack growth of edge and center cracks in façade rock panels subject to periodic surface temperature variations

K.T. Chau [a,*], J.F. Shao [b]

[a] *Department of Civil and Structural Engineering, The Hong Kong Polytechnic University, Yok Choi Road, Kowloon, Hung Hum, Hong Kong, China*
[b] *Laboratory of Mechanics of Lille, UMR 8107, CNRS, Polytech-Lille, Cite Scientifique, 59655 Villeneuve d'Ascq, France*

Received 13 October 2004; received in revised form 2 July 2005
Available online 30 August 2005

Abstract

This paper examines subcritical cracking in a rock panel or slab containing either a pre-existing edge or a center crack perpendicular to the panel surface. The panel is subject to periodic surface temperature variation on one side of the panel while the other is kept at a constant temperature. The thermally induced stress intensity factors are determined using superposition technique by employing the fundamental point load solution for an edge crack or a center crack in a slab of finite thickness. Rock panel is modeled as a long elastic strip with either a free or a fully constrained lateral end condition. The temperature variations versus time at various depths of the rock panel appear roughly as a sinusoidal function. The lateral thermal stress for the free end case is larger than the constrained end case; whereas stress intensity factors for both edge and center cracks in the constrained end slab are 1000 times larger than that of free end case. Subcritical crack propagation in rock panels on façade is then estimated as a function of time. This subcritical crack propagation continues until a critical crack size is attained and the rock panel will fail under wind load. This new theoretical framework provides a new paradigm to examine the mechanisms of time-dependent cracking in rock panels on façade of buildings.

Keywords: Periodic heating; Edge crack; Center crack; Rock slab; Subcritical crack growth

* Corresponding author. Tel.: +852 27666015; fax: +852 23346389.
E-mail address: cektchau@polyu.edu.hk (K.T. Chau).

0020-7683/$ - see front matter © 2005 Published by Elsevier Ltd.
doi:10.1016/j.ijsolstr.2005.07.010

1. Introduction

Rock panels or slabs on exterior cladding walls or façades of commercial buildings are subject to mechanical load due to wind pressure, thermal loads due to sunshine, and chemical effects (or stress corrosion) due to acid rain or polluted air. There have been numerous incidences of rock panel failure reported. A notable example is the Amoco Building (now Aon Center) in Chicago; and this case was well documented and has aroused international awareness on the safety and problem of cladding wall design (Trewhitt and Tuchmann, 1988; Anon., 1989; Ridout, 1989; Kent, 1990; Logan et al., 1993; Hook, 1994; Rudnicki, 2000). In 1985, bowing and cracking occurred on some 43,000 slabs of Italian Carrara marble (each of size 1.219 m × 0.9144 m) on the external façade of this 344 m tall 80-storey building. The replacement of cladding was completed in 1991 with a total cost of US$ 80 millions, which is exactly half of the total cost of the whole building about 20 years ago. In Hong Kong, serious spalling and cracking started to appear in the granite cladding to the 23-story Bank of East Asia head-quarter building at Des Voeux Road Central in 1993, 10 years after the building was completed. Since there was a risk of parts of the granite slabs falling off and endangering pedestrians, the Bank replaced the entire cladding, resulting in the loss of about HK$ 38 millions. The lawsuit of the Bank against the Architect and Sub-Consultant went all the way to the Court of Final Appeal. Another notable example is the warping of cladding marble panels of the Alvar Aalto's Finland Hall in Helsinki (Royer-Carfagni, 1999a,b). In the case of marble, thermal expansion anisotropy in calcite (which constitutes marbles) has been investigated by Widhalm et al. (1996), Royer-Carfagni (1999a,b), Leiss and Weiss (2000), Siegesmund et al. (2000) and Ferrero and Marini (2001); and this anisotropy is believed to lead to thermally induced bowing and strength degradation in Carrara marble. In particular, the difference in thermal expansion of grains of marble will lead to grain boundary damage; and in wet and cold weather water may penetrate into the grain texture and freeze, leading to greater damage and resulting in bowing of rock slabs. Because of this excessive bowing, subcritical crack growth may also take place in the fixtures of the panels. Such façade damages are much more frequent in the northern regions of the world, like Finland and Sweden, than in warm areas, like Sicily and Greece. Other examples of cracking problems in cladding can be found in the textbooks by Winkler (1975, 1994). For more information and potential problems on the use of stone in structures, the readers are referred to Winkler (1975, 1994), Lewis (1995), Franzini (1995), Chew et al. (1998), Smith (1999), Chacon (1999), Gauri and Bandyopadhyay (1999) and Bradley (2001).

Although stone or rock panels have been widely used in cladding all over the world, there is no international design standard for rock panels or slabs (Cohen and Monteiro, 1991; Ruggiero, 1995). There are some standard requirements on the testing of the mechanical properties of dimensional stone used in cladding, such as the CSIRO (Quick, 1998) and ASTM standards (e.g. C503-89; C880-89; C170-87). These tests normally include compressive strength, flexural strength, modulus of elasticity, density, absorption, thermal conductivity, coefficient of thermal expansion, creep deflection, and resistance to chemical agents. It will be shown in the present study that the end condition of the anchoring system used for holding the stones is of vital importance to the stability and cracking of rock panels, but no standardized anchoring system design has been adopted internationally. The main consideration for the design of anchors depends on its ability to resist wind and seismic loads, and to avoid bowing problems (Cohen and Monteiro, 1991). Stress concentrations between the connection and the rock panels are known to be highly dependent on the details of anchoring system (Ho and Chau, 1997, 1999; Chau and Wei, 2001). Although cracking is known to appear in cladding and dimensional stones (e.g. Simmons and Richter, 1993; Ayling, 2002), there is no theoretical study analyzing the cracking problem of rock panels under its normal working condition (i.e. the daily solar heating and wind load). This is the main objective of the present study.

The most likely failure mode of brittle rock panels is tensile cracking. The classical linear elastic fracture mechanics predict that as long as the stress intensity factor (SIF) at a crack tip is less than a critical value called fracture toughness (K_{IC}), the crack is stable and no crack propagation will occur. However, failure

cases (such as the Amoco case in Chicago and Bank of East Asia case in Hong Kong) and creeping experiments on rock specimens clearly show that crack propagation did occur even when the sustained SIF is less than K_{IC} as long as a threshold value is exceeded. This phenomenon is known as subcritical cracking (Atkinson, 1984; Atkinson and Meredith, 1987). Clearly, this kind of subcritical crack growth can provide a theoretical basis for long term cracking phenomenon of rock panels on cladding. For example, cracking of the Bank of East Asia cladding appeared only 10 years after its completion. Therefore, subcritical crack growth in rock panels in many existing and new structures deserves more detailed investigation. To examine time-dependent cracking and failure of rock panels on cladding wall, subcritical cracking resulting from periodic solar heating and wind loads is considered in the present study.

For the case of a two-dimensional body containing cracks, Rizk and Radwan (1992) considered the transient thermal stresses for both embedded and edge crack problems in half-planes. An edge crack in an elastic strip of finite thickness subject to sudden thermal transient stresses was considered by Rizk and Radwan (1993) and subject to convective cooling on the face containing the edge crack while the other face is insulated was considered by Rizk (1994). In these studies, numerical solution of singular integral equations is involved. None of these studies considered the case of a cracked strip subject to periodic temperature variations.

In the present study, we will consider the subcritical cracking of either an edge or a center crack in an elastic strip of finite thickness with both free and fully constrained end boundaries. One surface is subject to periodic temperature variation (i.e. simulated solar heating on rock panels) while the other is kept at a constant temperature (i.e. simulated constant indoor temperature in the building). Both of these edge and center cracks are assumed perpendicular to the surface of the elastic strip since this appears to be the most crucial situations. Physically, if a crack (either edge or center) is inclined to the strip surface, the temperature field is being disturbed across the thickness, at least around the crack, such that the temperature field is no longer one-dimensional. This occurs because a layer of air is expected to be trapped in the crack, which changes the uniformity of the conductivity across the thickness. Thus, the assumption of a perpendicular crack reflects the most crucial situation, and at the same time simplifies the problem mathematically. The problem is decomposed into two Associated Problems: (I) a noncracked strip subject to temperature variation shown in Fig. 1; and (II) a cracked strip subject to internal pressures that cancel those induced by Associated Problem I. The solution of Associated Problem I can be obtained from the treatise of Carslaw and Jaeger (1959). To avoid the use of singular integral equation formulation, we will employ the fundamental point force solution for an edge or a center crack in a strip of finite thickness to solve

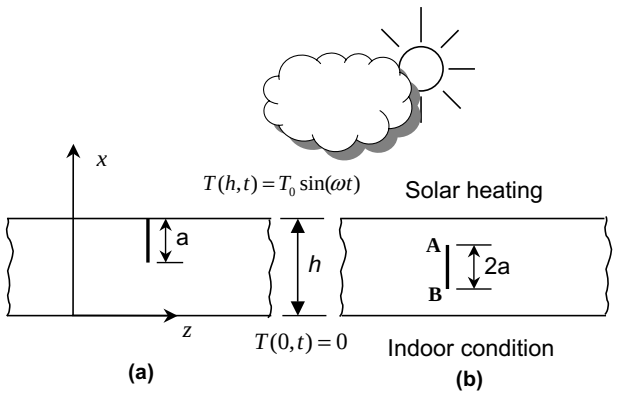

Fig. 1. Rock slabs subject to constant indoor temperature and periodic outdoor temperature variation induced by $T(h,t) = T_0 \sin(\omega t)$: (a) An edge crack of size a and (b) a center crack of size $2a$.

Associated Problem II. The pre-existing cracks are the smallest undetectable microcracks in the rock panels, while the critical crack length at which rock panel failure is expected is estimated from the bending of a cracked strip under wind load. The service life of these rock panels before severe cracking occurs can then be estimated as a function of time using the theoretical basis of fracture mechanics and subcritical crack propagation.

2. An elastic slab subject to periodic surface temperature

2.1. Temperature field in the slab

Consider a finite slab of thickness h subject to a periodic heating on the surface $x = h$ while the temperature is kept at constant on $x = 0$. If the coupling between the temperature field and the deformation is negligible, the heat conduction within the slab is governed by the standard diffusion equation (Carslaw and Jaeger, 1959)

$$\frac{\partial T}{\partial t} = \kappa \frac{\partial^2 T}{\partial x^2} \tag{1}$$

where T is the temperature and κ is the coefficient of diffusivity (about 0.01 cm^2/s for typical rocks, see Appendix VI of Carslaw and Jaeger, 1959). The boundary and initial condition of the slab are

$$T(0,t) = T_a; \qquad T(h,t) = T_0 \sin(\omega t + \varepsilon) + T_a \tag{2}$$

$$T(x,0) = T_a \tag{3}$$

where ε is the phase shift of the heating, ω is the circular frequency of temperature fluctuation ($= 2\pi(24 \times 60 \times 60) \approx 7.272 \times 10^{-5}\ s^{-1}$ for daily temperature variation), and T_0 is the magnitude of temperature fluctuation about the mean ambient room temperature T_a, which has been assumed to be spatially uniform. Note from the mathematical form of (1) that this T_a will not induce any temperature variation across the rock panel thickness. Typically for a subtropical region like Hong Kong, the room temperature is kept at 20 °C (on $x = 0$) while the external rock surface may rise to over 40 °C as a result of direct sun heating whereas it may drop to 15 °C at night. Thus, the magnitude of T_0 may be as large as 12 °C, while in the winter time the temperature fluctuation is somewhat smaller. We have assumed in (2) that the surface of the rock panel or slab is subject to periodic or daily solar heating such that a sinusoidal oscillation of the surface temperature is assumed on the external surface while the internal surface is kept at constant as prescribed by an air-conditioned interior. An alternative way to prescribe the boundary condition is to assume a background radiation plus a sinusoidal solar heating at daytime while only the background radiation at night (see Section 2.9 of Carslaw and Jaeger, 1959). However, the background radiation rate of a thin rock panel differs from that of the earth surface and is not known. Thus, this possibility will not be considered here.

The solution of (1) subject to (2) and (3) is given by Section 3.6 of Carslaw and Jaeger (1959) as

$$T(x,t) = T_0 \psi(x,t) + T_a \tag{4}$$

where

$$\psi(x,t) = \Omega(x) \sin[\omega t + \varepsilon + \phi(x)] + \frac{2\pi\kappa}{h^2} \sum_{n=1}^{\infty} \frac{n(-1)^n(\alpha_n \sin\varepsilon - \omega\cos\varepsilon)}{\alpha_n^2 + \omega^2} \sin\left(\frac{n\pi x}{h}\right) \exp(-\alpha_n t) \tag{5}$$

where $\alpha_n = \kappa n^2\pi^2/h^2$ and the amplitude $\Omega(x)$ and phase $\phi(x)$ of the temperature oscillations at point x are

$$\Omega(x) = \left\{\frac{\cosh(2kx) - \cos(2kx)}{\cosh(2kh) - \cos(2kh)}\right\}^{1/2}, \qquad \phi = \arg\left\{\frac{\sinh kx(1+i)}{\sinh kh(1+i)}\right\} \tag{6}$$

The heat wave number k and the imaginary constant i are defined by $[\omega/(2\kappa)]^{1/2}$ and $\sqrt{-1}$, respectively. The first term on the right hand side of (5) is the steady state periodic solution and the second is the transient term which dies out quickly with the summation index n. As shown in later section, the periodic term in (5) dominates the temperature field for the case of daily temperature on rock panels.

2.2. Elastic thermal stress

Consider a two-dimensional rock panel of large size along both and y- and z-directions and of a finite thickness h in the x-direction. A plane strain stress field can be assumed in the x–z plane shown in Fig. 1. The stress–strain relation with a temperature field T is

$$\begin{Bmatrix}\sigma_{xx}\\ \sigma_{zz}\\ \tau_{xz}\end{Bmatrix} = \begin{bmatrix}C_{11} & C_{13} & 0\\ C_{13} & C_{11} & 0\\ 0 & 0 & G\end{bmatrix}\begin{Bmatrix}\varepsilon_{xx}\\ \varepsilon_{zz}\\ 2\varepsilon_{xz}\end{Bmatrix} - \begin{Bmatrix}\lambda\\ \lambda\\ 0\end{Bmatrix}T \tag{7}$$

where σ_{xx}, σ_{zz}, and τ_{xz} are the normal stresses along the x- and z-directions and the shear stress along the z-direction on the x-plane, and G is the shear modulus. Similarly, the corresponding strain components are denoted by ε. The elastic moduli (C_{11} and C_{13}) and strain–temperature factor λ can be related to the Young's modulus (E), Poisson ratio (v) and coefficient of linear thermal expansion (α) as

$$C_{11} = \frac{(1-v)E}{(1-2v)(1+v)}, \quad C_{13} = \frac{vE}{(1-2v)(1+v)^2}, \quad \lambda = \frac{(1-v)\alpha E}{(1-2v)(1+v)} \tag{8}$$

For a two-dimensional slab with zero normal and tangential tractions on both the top and bottom, all strains will be zero except for ε_{zz}. Compatibility equation leads to the following form of ε_{zz}:

$$\varepsilon_{zz} = Ax + B \tag{9}$$

with A and B have to be determined by boundary condition, and all other strains in (7) are zero. Substitution of (9) into (7) leads to

$$\sigma_{zz} = C_{11}[A(t)x + B(t)] - \lambda T_0\psi(x,t) \tag{10}$$

where $T(x,t)$ is the temperature given in (4). Note that we can drop T_a in (10) if there is no thermal initial stress in the rock panel under ambient room temperature.

If the slab at $z \to \pm\infty$ is constrained, ε_{zz} will be identically zero which in turn leads to $A = B = 0$. But, in cladding design, the rock panels are normally separated by sealant, epoxy or cement paste so that a free boundary condition may be more appropriate. In particular, if the slab is free to expand and is moment free at $z \to \pm\infty$, the following constraints can be imposed:

$$\int_0^h \sigma_{zz}(x,t)\,dx = 0, \int_0^h x\sigma_{zz}(x,t)\,dx = 0 \tag{11}$$

Substitution of (10) into (9) yields two expressions for A and B, and solution of them gives

$$\begin{aligned} A(t) &= \frac{6T_0\gamma}{h}\left[\frac{2}{h}\int_0^h x\psi(x,t)\,dx - \int_0^h \psi(x,t)\,dx\right],\\ B(t) &= 2T_0\gamma\left[2\int_0^h \psi(x,t)\,dx - \frac{3}{h}\int_0^h x\psi(x,t)\,dx\right] \end{aligned} \tag{12}$$

where $\gamma = \lambda/(C_{11}h)$. Note that since the temperature field is a function of time, both A and B are functions of time as well. In reality, the actual end boundary condition of rock panels may be somewhere between free and fully constrained, depending on the detailing of the anchor system.

3. Stress intensity factors at cracked slab subject periodic surface temperature

In this section, two different crack problems in a slab of thickness h will be considered. The first one is an edge crack of size a shown in Fig. 1(a), while the second one is a center crack of size $2a$ shown in Fig. 1(b).

3.1. An edge crack in an elastic slab

Referring to Fig. 2(a), the mode I stress intensity factor induced by a pair of point loads P applied on the crack faces at c from the top free surface is given as (Tada et al., 1985)

$$K_{\mathrm{I}}^{E}(\xi,\eta) = \frac{2P}{\sqrt{\pi a}} F_{\mathrm{I}}(\xi,\eta) \tag{13}$$

where $\xi = c/a$ and $\eta = a/h$

$$F_{\mathrm{I}}(\xi,\eta) = \frac{3.52\xi}{(1-\eta)^{3/2}} - \frac{4.35 - 5.28(1-\xi)}{\sqrt{1-\eta}} + \left\{ \frac{1.3 - 0.3(1-\xi)^{3/2}}{\sqrt{\xi(2-\xi)}} + 0.83 - 1.76(1-\xi) \right\}(1-\xi\eta) \tag{14}$$

The solution given in (13) and (14) can be used as a fundamental solution for the crack problem shown in Fig. 1(a). By applying the principle of superposition, the crack problem subject to a temperature field given in (4) can be decomposed into two Associated Problems: (I) a noncracked slab subject to a temperature field given in (4); and (II) a cracked slab subject to an internal stress field which is generated on the position of the crack in Associated Problem I above. Since the stress field is not singular anywhere in the slab in Associated Problem I, only the Associated Problem II contributes to the calculation of the stress intensity factor at the crack tip. In particular, replacing P by $\sigma_{zz}^{*}(\xi,t)a\,\mathrm{d}\xi$ in (13) and integrating the result from 0 to 1, the following formula is obtained:

$$K_{\mathrm{I}}(\eta) = 2\sqrt{\frac{a}{\pi}} \int_0^1 \sigma_{zz}^{*}(\xi,t) F_{\mathrm{I}}(\xi,\eta)\,\mathrm{d}\xi \tag{15}$$

where

$$\sigma_{zz}^{*}(\xi,t) = \sigma_{zz}(\xi,t) = T_0\varphi(\xi,t) \tag{16}$$

It is clear from (12) and (4) that $A(t)$, $B(t)$ and $T(x,t)$ are all proportional to T_0, thus we can rewrite the stress term as $T_0\varphi(\xi,t)$ as given in (16).

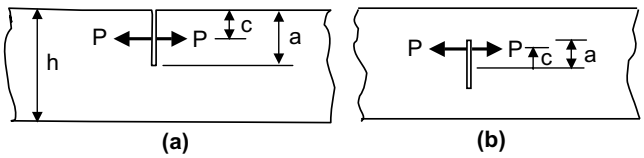

Fig. 2. Sketches for the fundamental problems of a pair of forces P applied to the crack faces in rock panel of thickness h: (a) edge crack and (b) center crack.

3.2. A center crack in an elastic slab

Referring to Fig. 2(b), the mode I stress intensity factor induced by a pair of point loads P applied on the crack faces at c from the center of the crack is given as (Tada et al., 1985)

$$K_{\mathrm{I}}^{C}(\xi,\eta)=\frac{1}{\sqrt{h}}F_{\mathrm{II}}(\xi,\eta)_{\pm 1} \tag{17}$$

where $\xi=c/a$, $\eta=a/h$ and

$$F_{\mathrm{II}}(\xi,\eta)_{\pm 1}=\left\{1+0.297\sqrt{1-\xi^2}[1-\cos(\pi\eta)]\right\}\sqrt{\tan(\pi\eta)}\frac{1\pm\sin(\pi\eta\xi)/\sin(\pi\eta)}{\sqrt{1-[\cos(\pi\eta)/\cos(\pi\eta\xi)]^2}} \tag{18}$$

The subscript "+1" is for the crack tip A while the subscript "−1" is for the crack tip B. The solution given in (17) and (18) can be used as a fundamental solution for the crack problem shown in Fig. 1(b). Similar to the discussion given in Section 3.1, we have

$$K_{\mathrm{I}}(\eta)=\frac{\sqrt{h}}{2}\int_{-2\eta}^{2\eta}\sigma_{zz}^{*}(\xi,t)F_{\mathrm{II}}(\xi,\eta)_{\pm 1}\,\mathrm{d}\xi \tag{19}$$

and the stress in the integrand of (19) has been defined in (16).

The integration of (15) and (19) can be done by following a standard procedure using an algorithm of Simpson's rule with error control (Press et al., 1992).

4. Numerical results for stress intensity factors

4.1. Selection of parameters

For external cladding wall design using rock panels, marble and other metamorphic rocks are normally used, but the use of granitic rocks are not uncommon. There are various sources on the mechanical and thermal parameters of marbles, especially Carrara marble (Bortz and Wonneberger, 1997; Mahmutoglu, 1998; Sglavo et al., 1999; Alber and Hauptfleisch, 1999; Cardani and Meda, 1999). Carrara marble had been the choice of structural stones since the time of Renaissances. The scientific research on the properties of marbles started in the last century, and more notable works include the classic triaxial tests conducted by von Karman in 1911 (Rudnicki, 2000; Jaeger and Cook, 1976) and the classic bowing experiments conducted by Rayleigh (1934). Thermal expansion anisotropy in calcite (which constitutes marbles) has been investigated by Widhalm et al. (1996), Royer-Carfagni (1999a,b), Leiss and Weiss (2000), Siegesmund et al. (2000) and Ferrero and Marini (2001); and this anisotropy is believed to lead to thermally induced bowing and strength degradation in Carrara marble. Microcracking properties in marbles were examined by Wong et al. (1995, 1996). Cyclic loading tests on Carrara marble have been conducted by Royer-Carfagni and Salvatore (2000).

In the following numerical examples, we have chosen some typical values of marble panels used for cladding walls: $E=35$ GPa, $\nu=0.27$, $\kappa=0.0118\ \mathrm{cm^2/s}$, $\alpha=1\times10^{-5}\ \mathrm{K^{-1}}$, $h=30$ mm, and $T_1=0.5$ day (or 43,200 s). Daily temperature fluctuations induced by solar heating are assumed. The corresponding heat conduction parameters are: circular frequency of temperature oscillations $\omega=2\pi/(24\times60\times60)\approx7.272\times10^{-5}\ \mathrm{s^{-1}}$, heat wave number $k=(\omega/2\kappa)^{1/2}=0.056$, and velocity of heat wave $(2k\omega)^{1/2}=0.0013$ cm/s (Carslaw and Jaeger, 1959).

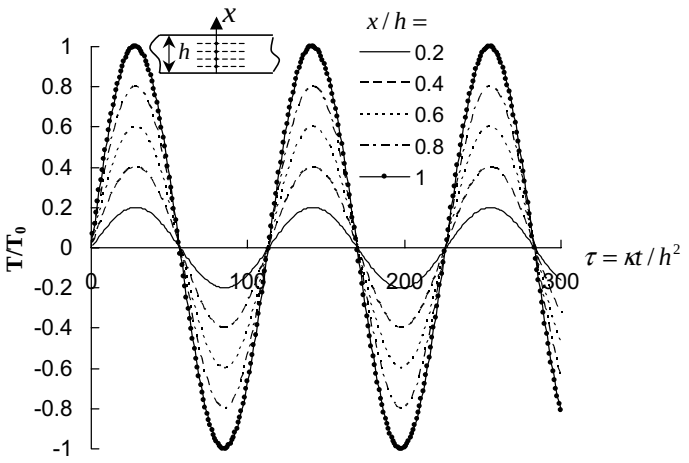

Fig. 3. The normalized temperature T/T_0 versus the normalized time $\tau = \kappa t/h^2$ at various depths of $x/h = 0.2$, 0.4, 0.6, 0.8 and 1.0. Note that the daily solar heating gives a periodicity of $\tau = 126$.

4.2. Temperature distribution in rock panels

Fig. 3 plots the temperature variations T/T_0 versus normalized time $\tau = \kappa t/h^2$ at various depths x/h (with $x/h = 1.0$ being on the external face of the rock panel and $x/h = 0.0$ being on the internal indoor face of the rock panel). Although the temperature solution given in (5) appears quite complicated, roughly periodic variations of temperature are obtained at all levels within the rock panel, with temperature decreasing monotonically from the external face to the internal face. These temperature variations can be used to calculate the thermally induced lateral stress given by (10) for both free and constrained ends.

4.3. Stress distributions within the rock panels

Fig. 4 plots the thermally induced stress $\sigma_{zz}/(\lambda T_0)$ versus the thickness x/h for various times ($0.5T_1$, T_1, $1.5T_1$ and $2T_1$, where $2T_1$ is the period of the temperature oscillation cycle) for both cases of free end (Fig. 4(b) and (c)) and constrained end (Fig. 4(a) and (d)). To make our plots more concise, the stress profiles at different times are grouped into the same plot. For example, the compressive and tensile stress profiles at $t = 0.5T_1$ and T_1 are plotted on Fig. 4(a), respectively; whereas, the stress profiles of much smaller magnitudes are grouped in Fig. 4(d). Similarly, the stress profiles for free ends are grouped in Fig. 4(b) and (c) for the stress profiles with large and small magnitudes, respectively. For daily solar heating, we have $T_1 = 0.5$ day (or 43,200 s). For the case of constrained ends, we found that no lateral stress is induced at the internal face at all time whilst the stress profile increases from zero to a roughly linear one at $t = 0.5T_1$ shown in Fig. 4(a); then this compressive stress profile becomes very small at $t = T_1$ with a peak at slightly above the mid-level (or $x/h \approx 0.6$) as shown in Fig. 4(d). For the case of free end rock slab, the stress profiles are quite different. Lateral stresses are not zero at the internal rock face because the rock slab is free to bend under this end condition. The maximum lateral stresses are about three times larger than those observed under the constrained end condition. It is also peculiar to see that there are two neutral points without stresses (at about $x/h \approx 0.2$ and 0.8) at times T_1 and $2T_1$. Once these stress profiles are obtained, (15) and (19) can be used to estimate the mode I stress intensity factors for edge and center cracks, respectively. The results are presented next.

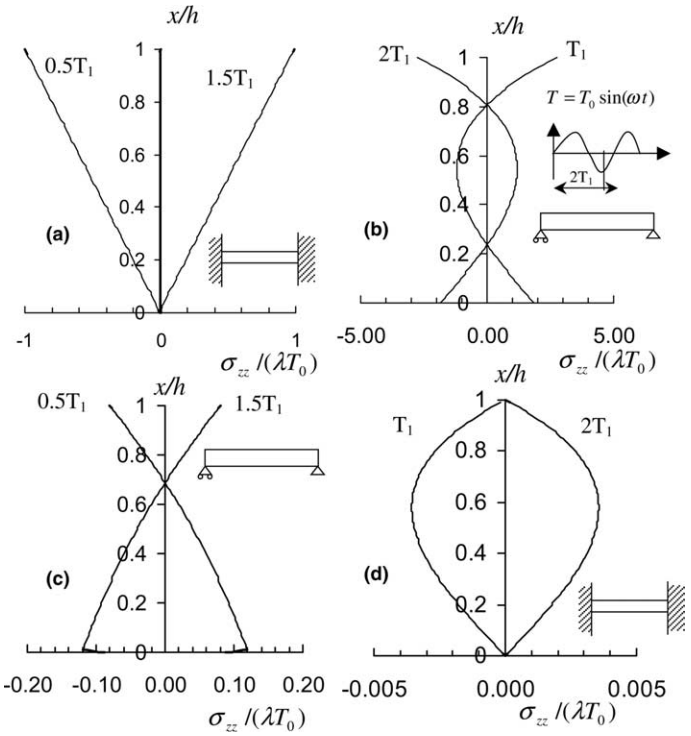

Fig. 4. The normalized thermal stress $\sigma_{zz}/(\lambda T_0)$ versus the thickness x/h for various times ($0.5T_1$, T_1, $1.5T_1$ and $2T_1$, where $2T_1$ being the period of the temperature oscillation cycle) for both cases of free end (in (b) and (c)) and constrained end (in (a) and (d)).

4.4. Stress intensity factors induced at crack tips

Fig. 5 plots the normalized stress intensity factor $K_1/[\lambda T_0\sqrt{(\pi a)}]$ versus the normalized time $\tau = \kappa t/h^2$ for both cases of edge crack and center crack (both tips A and B shown in Fig. 1). The numerical results are for a slab containing a crack of size $a/h = 0.25$ (for both edge and center crack cases). The results for rock slabs with constrained ends are shown in Fig. 5(a) whereas those for free end are shown in Fig. 5(b). It should be noted that the magnitudes of the stress intensity factor for free end cases are about three orders of magnitude smaller than those of the constrained end cases. This occurs because, as shown in Fig. 4(b) and (c), although the stress magnitude is larger for free end cases, there are both compressive and tensile stresses appearing simultaneously across the thickness at any particular time whereas the stress profiles are either all compressive or all tensile at any instance of time for the constrained case. As shown in Fig. 5(a), all the stress intensity factors are in phase for the case of constrained end, with the largest stress intensity factors occurring for edge crack followed by those of crack tips A and B of the center crack case. Note also the compressive stress intensity factors have been cut off, showing only the tensile or crack opening cases. Fig. 5(b) shows that there remains a compressive cut off zone for the case of center crack, but there is no compressive cut off zone in the edge crack case. In addition, there is a clear phase shift of T_1 in Fig. 5(a) and (b). That is, stress intensity factor builds up instantly at $\tau = 0$ for the case of free end; but there is a time delay in the stress intensity factor for constrained end.

The results of this section will be used next in subcritical crack growth consideration.

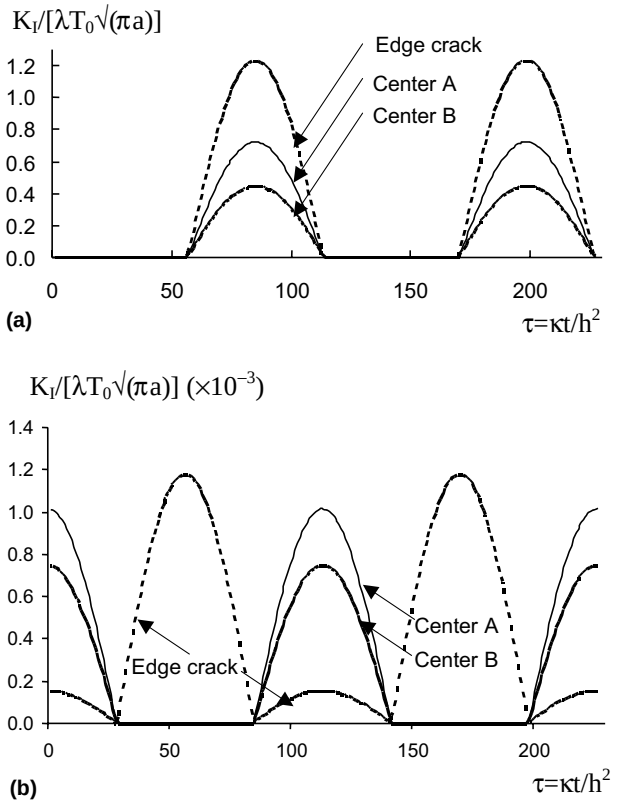

Fig. 5. The normalized stress intensity factor $K_I/[\lambda T_0\sqrt{(\pi a)}]$ versus the normalized time $\tau = \kappa t/h^2$ for both edge crack and center crack: (a) constrained end condition for rock panel and (b) free end condition for rock panel. The crack length is set at $a/h = 0.25$. The "center A" represents the solution at crack tip A for the center crack shown in Fig. 1, whereas "center B" for crack tip B shown in Fig. 1.

5. Subcritical crack propagation due to the thermal stress

5.1. Combined fatigue and subcritical crack growth

In the present problem, periodic loading and unloading at crack tips occur because of the periodic temperature rise and drop. Thus, fatigue–crack growth may also be induced, which cannot be modeled by the subcritical crack growth alone. As discussed by Hertzberg (1996), it possible to incorporate both fatigue and subcritical crack growths:

$$\left(\frac{da}{dN}\right)_T = \left(\frac{da}{dN}\right)_{Fat} + \int \frac{da}{dt} K(t)\, dt \tag{20}$$

where a and N are the crack length and number of loading cycle, and subscripts "T" and "Fat" denote the total and the fatigue–crack growth. First of all, cyclic loading tests under reference environment (i.e. an environmental with no observable stress corrosion crack growth) are performed at a certain stress intensity factor level. Then, at the same stress level, a sustained loading experiment can be conducted to yield information on stress corrosive cracking (or subcritical cracking). Unfortunately, such a two sequence experiment has

not been conducted for rocks in the laboratory, except for the cyclic fatigue–crack propagation for sapphire conducted by Asoo et al. (2000). Because subcritical crack growth in rocks was mainly studied in the context of geophysics and geology, fatigue cracking in rock has largely been neglected. Due to the lack of experimental data, only subcritical crack growth is considered next.

5.2. Subcritical crack growth

Linear elastic fracture mechanics predicts that once the stress intensity factor K_I at a crack tip of crack size a in an elastic body attains the so-called critical stress intensity factor K_{IC} or fracture toughness, crack propagation occurs or the crack size a increases. Whether the crack propagation will continue depends on the variation of K_I with the increasing value of a. This classical theory predicts that there will be no crack growth as long as $K_I < K_{IC}$. For real geological materials such as rock, however, the local stress field around the rock is highly nonuniform at the grain scale; and more importantly, the mechanical properties of grains around the crack tip degrade gradually because of the presence of water or other chemically agents inside the crack when the crack is propped open (i.e. stress corrosion). Numerous experimental results show that when these materials are subject to long term loading, they show considerable rates of macroscopic crack extension at values of K_I significantly lower than K_{IC}. This is called static fatigue or more commonly known as subcritical crack propagation (Atkinson, 1984).

As discussed by Atkinson (1984) and Atkinson and Meredith (1987), the following well-known Charles (1958) power law has been used widely to describe the subcritical crack growth in geological materials:

$$\frac{da}{dt} = v_0 \exp\left(-\frac{H}{RT}\right) K_I^n \tag{21}$$

where H is the activation enthalpy, R is the gas constant ($\approx$08.314472 J mol^{-1} K^{-1}), and T is the absolute temperature. The constants v_0 and n depends on both rock type and environmental effect, such as temperature, moisture, and chemical content in air; and n is also called stress corrosion or subcritical crack growth index. For diffusion controlled crack growth, n is about 2–10; while for stress corrosion crack growth, n is about 20–50. Another simplified form of (21) has been used by many authors (e.g. Miura et al., 2003)

$$\frac{da}{dt} = V_0 \left(\frac{K_I}{K_0}\right)^n \tag{22}$$

where V_0 is the crack velocity at $K_I = K_0$, and $K_0 < K_I < K_{IC}$. Experimental data for ceramics suggests that n is not a constant but changes with K_I; and, in general, three regions of crack propagation behavior are observed. For small K_I, da/dt is mainly controlled by the rate of stress corrosion reactions at the crack tips ($n \approx 2$–10); for larger K_I, da/dt is controlled by the rate of transport of reactive species to crack tips ($n \approx 0$); and finally for K_I close to K_{IC}, da/dt is controlled by thermally activated bond rupture which is largely independent of chemical environment ($n \approx 20$–50). For most rocks under room temperature and pressure, only region one or three is apparent (Atkinson, 1984).

For the present crack problems of rock panels subject to daily solar heating, K_I is clearly a function of time and temperature at the crack tip always varies with time. Thus, in general, we should use (21) instead of (22). However, we will not do so for two reasons: first, v_0 is not given in Atkinson (1984) and the variation of temperature is not very significant comparing to other constants in the exponential term in (21).

5.3. Crack length as a function of time

Once K_I is known as a function of time, (22) can be integrated to yield the crack length as a function of time. Instead of integrating (22) exactly, an approximate formula is normally used. For example, we note that the stress intensity factor for the center crack case can be rewritten in the classical form as

$$K_{\mathrm{I}} \approx YT_0\sqrt{\pi a}\int_0^1 \varphi(\xi,t)F_{\mathrm{I}}(\xi,\eta)\,\mathrm{d}\xi \tag{23}$$

for some constants Y. Furthermore, the size of crack only appears in the dimensionless ratio η in (23) and thus we further assume that the integral term in (23) is independent of the crack size a. Making this assumption, substituting either (15) or (19) into (22), and integrating the resulting equation leads to

$$a(t) \approx \left\{a_0^{(2-n)/2} + \frac{(2-n)}{2}V_0\left(\frac{2T_0}{\sqrt{\pi}K_0}\right)^n \int_0^t \Phi^n(\tau,\eta)\,\mathrm{d}\tau\right\}^{2/(2-n)} \tag{24}$$

where

$$\Phi(t,\eta) = \int_0^1 \varphi(\xi,t)F_{\mathrm{I}}(\xi,\eta)\,\mathrm{d}\xi \tag{25}$$

for the edge crack. For the case of center crack, by noting that the first order term of the expansion of $[\tan(\pi\eta)]^{1/2}$ (which can be found in the definition of F_{II} given in (18)) is proportional to $(a/h)^{1/2}$ and following a similar argument we can also arrive at (24) with $\Phi(t,\eta)$ being replaced by

$$\Phi(t,\eta) = \frac{1}{4}\sqrt{\frac{\pi h}{a}}\int_{-2\eta}^{2\eta} \varphi(\xi,t)F_{\mathrm{II}}(\xi,\eta)\,\mathrm{d}\xi \tag{26}$$

In (24), initially a_0 can be interpreted as the largest undetectable initial crack size, and for geological materials it is typically of the dimension of the grain size of minerals constituting the rocks; and the upper limit of integration should not be too large and $\Phi(t,\eta)$ should be updated regularly as a increases.

5.4. A simplified subcritical crack growth model

Instead of assuming the classical form of (24), we can also integrate (22) directly as

$$a(t) = a_0 + \int_0^t V_0\left[\frac{K_{\mathrm{I}}(\zeta)}{K_0}\right]^n \mathrm{d}\zeta \tag{27}$$

provided that $K_{\mathrm{I}}(t)$ as a function of time is known. Fig. 5 suggests that $K_{\mathrm{I}}(t)$ can be approximated as some "upper-sine-function" with periodicity of $2T_1$. Therefore, to simplify the numerical integration two different cases of integration can be used.

Case I

For case I, an upper-sine-function can be used to approximate the stress intensity factors versus time within one period $2T_1$. As shown in Fig. 7(a) and (b), this case is appropriate for edge crack with constrained end and for center cracks with both free and constrained ends. In particular, $K_{\mathrm{I}}(t,\eta)$ can be approximated as

$$\begin{aligned} K_{\mathrm{I}}(t,\eta) &= K_{\max}\sin\left(\frac{\pi t}{T_1}\right) \quad T_1 + T_{00} < t < 2T_1 - T_{00} \\ &= 0 \quad \text{all other time} \end{aligned} \tag{28}$$

where $K_{\max} > K_0$ and $2T_1 > t > 0$ (see Fig. 7), and we have defined

$$T_{00} = \frac{T_1}{\pi}\sin^{-1}\left(\frac{K_0}{K_{\max}}\right) \tag{29}$$

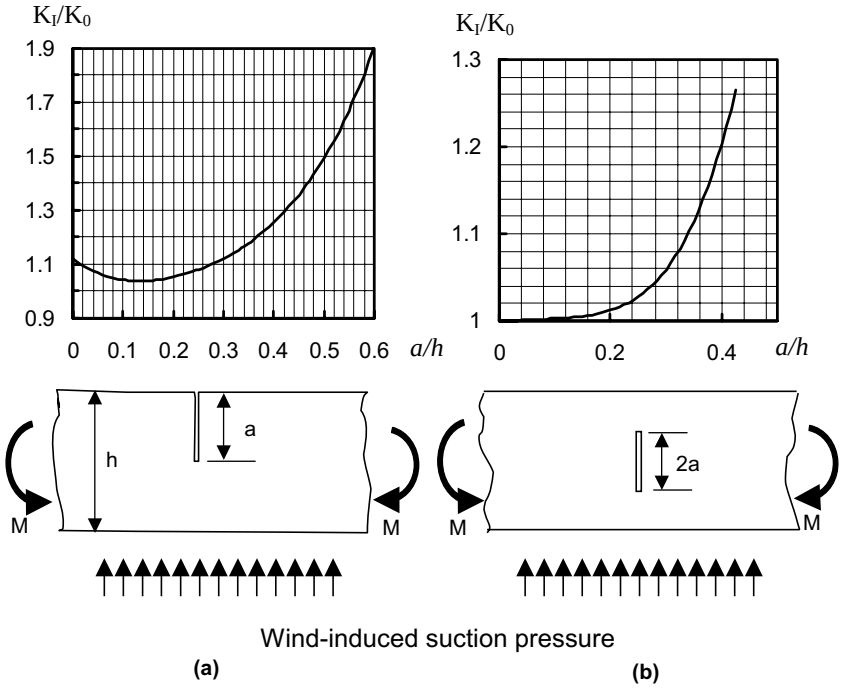

Fig. 6. The stress intensity factors K_I/K_0 versus a/h for a crack in a slab of thickness h subject to bending moment M (which is assumed being induced by wind suction as illustrated): (a) edge crack and (b) center crack. Approximate formulas for these curves are given in (33) and (34).

Case II

For case II, as shown in Fig. 7(c), the case of edge crack with free ends, $K_I(t,\eta)$ can be approximated as

$$\begin{aligned} K_I(t,\eta) &= K_{\max 1}\sin\left(\frac{\pi t}{T_1}\right) \quad T_{01} < t < T_1 - T_{01} \\ &= K_{\max 2}\left|\sin\left(\frac{\pi t}{T_1}\right)\right| \quad T_1 + T_{02} < t < 2T_1 - T_{02} \end{aligned} \tag{30}$$

where both $K_{\max 1}$ and $K_{\max 2}$ are larger than K_0 and $2T_1 > t > 0$. In addition, T_{01} and T_{02} can be obtained by replacing $K_{\max}$ with $K_{\max 1}$ and $K_{\max 2}$ in (29), respectively. Note that we have to exclude the contribution of $K_I(t,\eta)$ if K_I is smaller than K_0. Substitution of (28) or (30) into (27) and integration of the result over one day period, we have the following approximation for the subcritical crack growth for Case I (shown in Fig. 7(a) and (b)):

$$a(2T_1) = a_0 + V_0\left(\frac{K_{\max}}{K_0}\right)^n \int_{T_{00}}^{T_1 - T_{00}} \sin^n\left(\frac{\pi\zeta}{T_1}\right)\mathrm{d}\zeta \tag{31}$$

where T_1 equals half a day in our problem. For integration of Case II shown in Fig. 7(c), we have

$$a(2T_1) = a_0 + V_0\left\{\left(\frac{K_{\max 1}}{K_0}\right)^n \int_{T_{01}}^{T_1 - T_{01}} \sin^n\left(\frac{\pi\zeta}{T_1}\right)\mathrm{d}\zeta + \left(\frac{K_{\max 2}}{K_0}\right)^n \int_{T_{02}}^{T_1 - T_{02}} \sin^n\left(\frac{\pi\zeta}{T_1}\right)\mathrm{d}\zeta\right\} \tag{32}$$

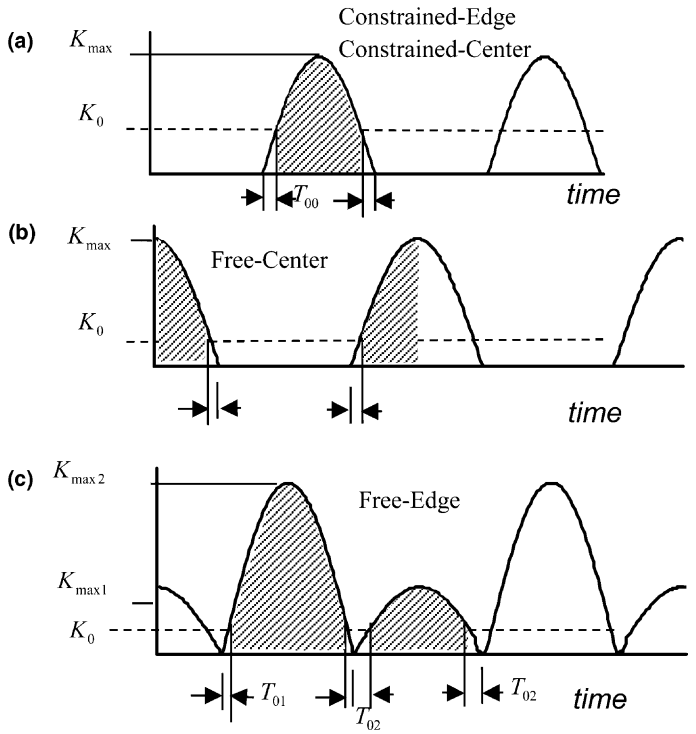

Fig. 7. A sketch illustrating the integration for subcritical crack propagation: (a) constrained end for both edge and center crack; (b) center crack with free end and (c) edge crack with free end. The threshold stress intensity factor is denoted by K_0. Subcritical cracking is estimated from the hatched areas in the plots.

Since the crack growth rate is very slow for subcritical crack propagation, the dependence of K_{max} with the crack size $a(t)$ is expected to be small within duration of days, as shown in Fig. 7. Thus, we can use the estimation of (34) and (35) for crack growth for a period of a day before we update the calculation of $K_{max}(a)$, $T_{00}(a)$, $T_{01}(a)$, and $T_{02}(a)$ as function of the current crack size. Using this simplified scheme, the subcritical crack growth for years can be estimated efficiently. The numerical calculation of the subcritical crack growth of pre-existing crack is conducted until the crack size equal to a critical size a_c which will be discussed next.

5.5. Determination of the critical crack size

For structural engineers and architects, the main design criterion for rock panels mounted on the façade of a building is wind load. Both outdoor wind pressure and the corresponding indoor suction pressure mainly induce bending stress in the rock panels. To make our problem mathematically tractable, the bending moment at the mid-span of the rock panel is first estimated using simple beam theory. Then, the stress intensity factor at the crack of a given size a is estimated by that of a thin slab containing either an edge or center crack subject to bending moment M at the supports (see Fig. 6). The stress intensity factor for the case of edge crack is given as (pp. 86–87 of Rooke and Cartwright, 1976)

$$K_I = \frac{6M\sqrt{\pi a}}{h^2}\Gamma_E(\eta) = \frac{6M\sqrt{\pi a}}{h^2}\left\{1.12 - 1.39\eta + 7.32\eta^2 - 13.1\eta^3 + 14\eta^4\right\} \tag{33}$$

where η is again defined as a/h; and for the case of center crack as (pp. 12–13 of Rooke and Cartwright, 1976)

$$K_{\mathrm{I}} = \frac{6\eta M\sqrt{\pi a}}{h^2}\Gamma_{\mathrm{C}}(\eta) = \frac{6\eta M\sqrt{\pi a}}{h^2}\left\{1 + 0.0148\eta + 0.2728\eta^2 - 2.7912\eta^3 + 12.9776\eta^4\right\} \tag{34}$$

Eq. (34) was obtained by fitting the curve given on p. 13 of Rooke and Cartwright (1976), which is valid only for $\eta < 0.425$. Both (33) and (34) are also plotted in Fig. 6 for the sake of completeness. For free boundary condition at the end of the rock slab, we have $M = wL^2/8$ and for constrained boundary condition, we have $M = wL^2/24$. Setting K_{I} equal to the fracture toughness K_{IC}, a as a_{c} and $\eta_{\mathrm{c}} = a_{\mathrm{c}}/h$ in either (33) or (34), we obtain the following critical crack size:

$$a_{\mathrm{c}} = \frac{1}{\pi}\left[\frac{h^2 K_{\mathrm{IC}}}{6M\Gamma_{\mathrm{E}}(\eta_{\mathrm{c}})}\right]^2 \quad \text{and} \quad a_{\mathrm{c}} = \frac{1}{\pi}\left[\frac{h^2 K_{\mathrm{IC}}}{6\eta_{\mathrm{c}} M\Gamma_{\mathrm{C}}(\eta_{\mathrm{c}})}\right]^2 \tag{35}$$

for edge crack and center crack, respectively. Note that these expressions have to be solved by iteration as the unknown a_{c} also appears in η_{c} on the right hand side of the equation.

As an illustration, we can set the wind suction per meter as 3.5 kN/m (i.e. $w = 3.5$ kN/m), which corresponds the largest design wind pressure for building at elevation of higher than 100 m in Hong Kong (BDD, 1983), the length of the rock slab as 1.5 m (i.e. $L = 1.5$ m) (which is comparable to the size used in Amoco Building), $h = 3$ cm (which is a typical thickness for rock slab used in façade), and $K_{\mathrm{IC}} = 0.64$ MPa m$^{1/2}$ (for Carrara Marble from Atkinson, 1984). For free boundary, the critical crack size a_{c} for edge and center cracks are 0.28 cm and 1.22 cm; while for constrained boundary, a_{c} for edge crack is 1.4 cm while no solution can be found for $\eta < 0.425$ for center crack. Thus, a crack of considerable depth has to be formed before catastrophic failure can occur under wind load.

5.6. Numerical results and discussion

In this section, numerical simulations of subcritical crack growth on rock panel caused by daily solar heating are conducted. Carrara marble is considered here as an example. The power index n is estimated as 18, which was obtained by Atkinson (1984) for specimens tested in air at 20 °C with a relative humidity of 30%. In addition, the fracture toughness is $K_{\mathrm{IC}} = 0.64$ MPa m$^{1/2}$ (Atkinson, 1984), and the initial pre-existing crack size is set to 0.0002 m or 0.2 mm which is the order of the grain size of calcite in marble (Wong et al., 1995, 1996). The daily temperature fluctuations in many parts of the world can vary significantly from summer to winter. We assume that a daily fluctuation in temperature of 15 °C (i.e. $T_0 = 7.5$ K in (2)). The value appears to be a bit large in terms of daily temperature fluctuation. However considering the fact that the temperature rise on rock surface under direct sunshine can be significantly larger than the surrounding ambient air temperature, this value is not unreasonable.

Fig. 8 plots the normalized crack length a/a_0 versus time for different kinds of crack and boundary conditions. The crack velocity at K_0, the threshold value of K, is set at 1×10^{-12} m/s. Note that the threshold K_0 chosen for the case of free-center crack, fixed-edge crack, free-edge crack and fixed-center crack are $0.00013K_{\mathrm{IC}}$, $0.13K_{\mathrm{IC}}$, $0.00036K_{\mathrm{IC}}$, and $0.06K_{\mathrm{IC}}$, respectively. These values are chosen such that subcritical crack propagation becomes possible (i.e. $K_{\mathrm{I}} < K_{\mathrm{IC}}$ for each case). If the chosen K_0 is too large, there is no subcritical crack propagation. If the chosen K_0 is too small, subcritical crack propagation may grow rapidly and cracking through the thickness may be completed within a few days (considering the exponential power of about 18 in (22)). Therefore, a larger value of K_0 chosen in Fig. 8 indicates a more favorable condition for subcritical crack growth. As suggested by Fig. 8, the case of an edge crack subject to the fixed end condition is most conducive to subcritical crack growth; and thus fixed end condition should be avoided in practice when anchoring system is designed. The free end conditions appear to be more resistant to

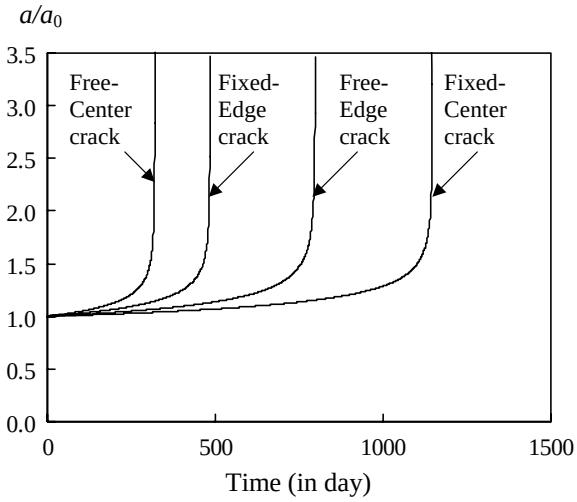

Fig. 8. The normalized crack length a/a_0 versus time (in days) for various types of crack and boundary conditions. The threshold values K_0 used for the cases of free-center crack, fixed-edge crack, free-edge crack and fixed-center crack are $0.00013K_{IC}$, $0.13K_{IC}$, $0.00036K_{IC}$, and $0.06K_{IC}$, respectively. Other parameters used in this plot are $V_0 = 10^{-12}$ m/s, $h = 3$ cm, $a_0 = 0.02$ cm, $K_{IC} = 0.64$ MPa $m^{1/2}$, $E = 35$ GPa, $v = 0.27$, $\kappa = 0.0118$ cm^2/s, $\alpha = 1 \times 10^{-5}$ K^{-1}, $K_0 = 0.13K_{IC}$, $n = 18$, $T_0 = 7.5$ °C and $T_1 = 0.5$ day (or 43,200 s).

subcritical crack growth. For the case of marble slabs, free end condition may be more conducive to thermally induced bowing; whereas, as shown in the present study, fixed end condition is more conducive to subcritical crack growth. Therefore, we must strike a balance in designing for an anchoring system to avoid both bowing and cracking problems. It was reported by Atkinson and Meredith (1987) that subcritical crack growth is known to exist in rocks for a threshold K_0 as small as $0.05K_{IC}$. Thus, our chosen values may be not unrealistic. Note, however, the crack growth rate V_0 may vary for different levels of K_I (Atkinson, 1984), but such complication will not be considered here. For the most critical case of fixed-edge crack, it takes 487 days for a pre-existing edge crack of 0.2 mm to grow to a critical crack size of 1.4 cm estimated in Section 5.5. Considering that only one third of the year has sunshine leading to the assumed temperature fluctuation given in (2) on the rock panels, it takes about four years for the edge crack to grow to a critical value. If K_0 increases slightly from $0.13K_{IC}$ to $0.135K_{IC}$, it takes about 982 days for the final cracking failure (see also Fig. 11). Following the same argument, this leads to about eight years for the edge crack to grow to the critical value. This value is comparable to the time of observation of serious spalling and cracking reported in the case of Bank of East Asia Head-quarter Building in Hong Kong in 1993 and of Amoco Building in Chicago in 1985.

It should be noted that crack growth rate is rather gradual and steady in the initial phase, then grows exponentially in the last few months of this subcritical crack propagation. For example, for the fixed-edge crack growth shown in Fig. 8, the crack sizes are about 0.3 mm, 0.4 mm, 0.5 mm, 0.7 mm and 1.4 mm at about 464, 482, 484, 485, and 487 days, respectively. Therefore, the subcritical crack growth theory suggests that there is not much precursory cracking before the final failure of the rock panel due to subcritical cracking. Therefore, this makes the regular visual inspection of the cracking on rock panel surface extremely difficult and ineffective, and perhaps some better ways should be developed to monitor the subcritical cracking on rock panels on cladding.

Since the fixed-edge crack case is most crucial in terms of cracking in rock panels on cladding or façade subject to periodic surface temperature variation, such case will be used in the following parametric studies.

Fig. 9 plots the normalized crack length a/a_0 versus time for various crack growth velocity V_0 (= 5, 1.5, 1, 0.8 and 0.6×10^{-12} m/s) for the case of fixed-edge crack. As expected, a longer time is needed for the subcritical cracking to reach a critical value for a smaller crack growth velocity V_0. It is observed that the time for reaching the stage of critical cracking (corresponding to the vertical growth of da/dt in Fig. 9) increases nonlinearly with the decrease of V_0. Although (22) suggests a linear variation of da/dt with V_0, actually K_I is a nonlinear function of the crack length a, and this results in a nonlinear behavior of da/dt versus V_0. When V_0 decreases from 5×10^{-12} m/s to 0.6×10^{-12} m/s, the time to failure increases nonlinearly from 102 days to 808 days. Therefore, the exact time of failure is very sensitive to the parameters of the subcritical cracking law given in (22).

Fig. 10 plots the normalized crack length a/a_0 versus time for various values of the exponent n (= 16, 18, 20, and 22) for the case of fixed-edge crack. A higher value of n in (22) implies a larger increase of the crack growth rate, thus, as expected, a shorter time to failure is observed for a larger n. The time of failure increases from 286 days to 650 days when n decreases from 22 to 16. As discussed earlier, for real rocks there may be three different regions of crack growth rate, depending on the operating subcritical crack growth mechanism. That is, for stress corrosion controlled cracking, we have $n \approx 2$–10; for transport rate controlled cracking, $n \approx 0$; and for thermally activated bond rupture cracking, we have $n \approx 20$–50. Atkinson (1984) reported that obvious decrease in n value versus K_I is only observed experimentally for synthetic quartz tested at 200 °C, and for sapphire tested in nitrogen atmosphere. There is no specific variation of n versus K_I of marble or granite at our operating temperature. Therefore, we will not consider the possibility of n changing with K_I in the present study.

Fig. 11 plots the normalized crack length a/a_0 versus time for various values of K_0/K_{IC} (= 0.125, 0.13, 0.138, 0.142 kPa $m^{1/2}$) for the case of fixed-edge crack. The time of failure increases from 241 days to 2821 days when K_0/K_{IC} increases from 0.125 to 0.138. For the present case shown in Fig. 11, the initial thermally induced stress intensity factor K_I/K_{IC} equals 0.14436 for $a_0 = 0.2$ mm. When K_0/K_{IC} is too small such that $K_I < K_0$, there will be no subcritical crack growth. When K_0/K_{IC} is too large such that $K_I \gg K_0$, subcritical crack growth may lead to cracking through the thickness in a matter of days, and thus cannot explain the field observation. For example, if we further decreases K_0/K_{IC} to 0.12, 0.11 and 0.1 kPa $m^{1/2}$, the time to

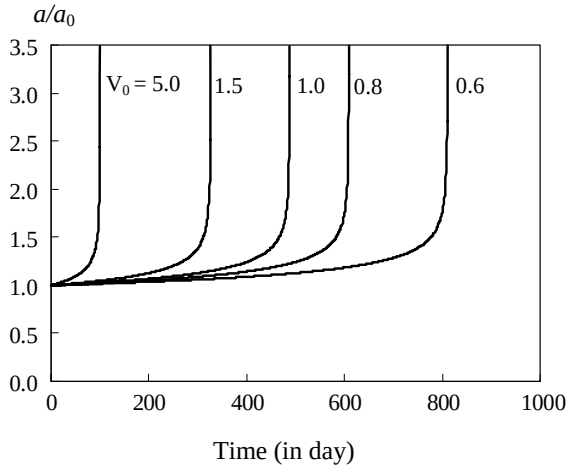

Fig. 9. The normalized crack length a/a_0 versus time (in days) for various values of V_0 for the fixed-edge crack. All values of V_0 shown should be multiplied by 10^{-12} m/s. Other parameters used in this plot are: $h = 3$ cm, $a_0 = 0.02$ cm, $K_{IC} = 0.64$ MPa $m^{1/2}$; $E = 35$ GPa, $\nu = 0.27$, $\kappa = 0.0118$ cm^2/s, $\alpha = 1 \times 10^{-5}$ K^{-1}, $K_0 = 0.13K_{IC}$, $n = 18$, $T_0 = 7.5$ °C and $T_1 = 0.5$ day (or 43,200 s). The plots are for subcritical crack propagation of an edge crack in a slab with fixed end.

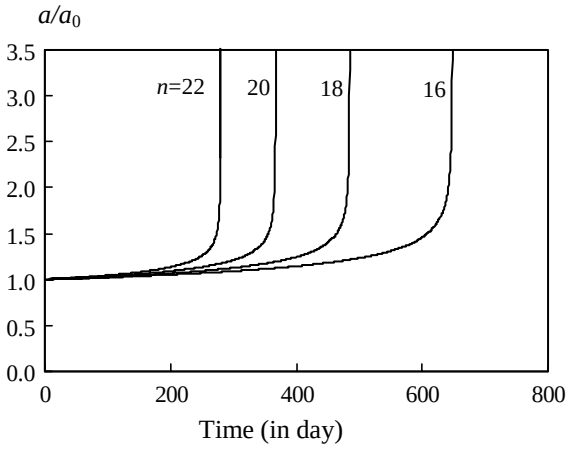

Fig. 10. The normalized crack length a/a_0 versus time (in days) for various values of n or edge crack with fixed boundary condition. Other parameters used in this plot are the same as those for Fig. 9, except for $V_0 = 10^{-12}$ m/s.

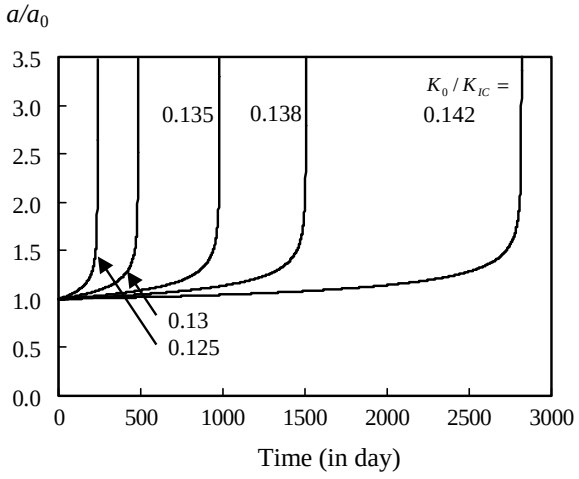

Fig. 11. The normalized crack length a/a_0 versus time (in days) for various values of K_0/K_{IC} for the fixed-edge crack case. Other parameters used in this plot are the same as those for Fig. 8, except for $V_0 = 10^{-12}$ m/s.

failure drops rapidly to 118, 28 and 8 days, respectively. Therefore, subcritical crack growth rate is extremely sensitive to the value of threshold K_0/K_{IC}.

6. Conclusions

This paper presents a framework to analyze subcritical cracking in rock panels containing either a pre-existing edge or center crack perpendicular to the panel surface subject to periodic surface temperature variation on one side of the panel while the other is kept at constant temperature. The thermally induced stress intensity factors are determined using superposition technique by employing the fundamental point loads solution for an edge crack or a center crack in a slab. Rock panels are modeled as a long elastic strip with

either free or fully constrained end condition. The temperature variations versus time at various depths of the rock panels appear roughly as sinusoidal functions. The lateral stress for the free end case is larger than the constrained end case; whereas the stress intensity factors for crack in constrained end slab are thousand times larger than that of free end case. Subcritical crack propagation in rock panels on façade is then estimated as a function of time. Carrara marble has been selected as an example to illustrate subcritical cracking. Subcritical crack propagation continues until a critical crack size is attained at which rock panel will fail under wind load. The subcritical crack growth rate is found very sensitive to the crack velocity, the exponential power, and the threshold stress intensity factor in the Charles' law.

Cracking through the thickness of the rock panels can complete in a matter of days or years, depending on the parameters used in the subcritical cracking law. This time-dependent cracking phenomenon provides a plausible explanation for the observed cracking phenomenon for the 1993 case of Bank of East Asia in Hong Kong and other cases. In short, this study should provide a new fracture-mechanics-based framework to analyze and design rock panels used in external façade of modern buildings, through the use of time-dependent subcritical cracking in rock panels. Since our preliminary results show that the time-dependent cracking depends strongly on the parameters of subcritical crack law, more refined experimental study is needed to determine these parameters as a function of the water vapour content and chemical contents in polluted air to which these rock panels are subject to.

Acknowledgements

The work has been supported by a grant from the *PROCORE*—France/Hong Kong Joint Research Scheme sponsored by the Research Grants Council of Hong Kong and the Consulate General of France in Hong Kong (Reference No. F-HK24/02T or PolyU No. 3-ZF81). This research was initiated in the summer of 2003 when KT Chau was visiting the Laboratory of Mechanics of Lille, France, and was completed in the summer of 2004 again in Lille. The later part of this study was fully supported by a grant from the Research Grants Council of the Hong Kong Special Administrative Region, China (Project No. PolyU 5166/04E).

References

Alber, M., Hauptfleisch, U., 1999. Generation and visualization of microfractures in Carrara marble for estimating fracture toughness fracture shear and fracture normal stiffness. International Journal of Rock Mechanics and Mining Sciences 36, 1065–1071.

Anon., 1989. Granite will replace old marble on Amoco façade. Civil Engineering 59 (6), 19–20.

Asoo, B., McNaney, J.M., Mitamura, Y., Ritchie, R.O., 2000. Cyclic fatigue–crack propagation in sapphire in air and simulated physiological environments. Journal of Biomedical Materials Research 52 (2000), 488–491.

Atkinson, B.K., 1984. Subcritical crack growth in geological materials. Journal of Geophysical Research 89 (B6), 4077–4114.

Atkinson, B.K., Meredith, P.G., 1987. The theory of subcritical crack growth with applications to minerals and rocks. In: Atkinson, B.K. (Ed.), Fracture Mechanics of Rocks. Academic Press, London, pp. 111–166.

Ayling, L., 2002. A solution for the stone repair of a cracked primary column at the Wellington Arch, Hyde Park Corner, London. In: Fidler, J. (Ed.), Stone–Stone Building Materials, Construction and Associated Component Systems: Their Decay and Treatment, James & James, London.

Building Development Department (BDD), 1983. Code of Practice on Wind Effects, Hong Kong-1983. Building Development Department, Hong Kong.

Bortz, S.A., Wonneberger, B., 1997. Laboratory evaluation of building stone weathering. In: Labuz, J.F., (Ed.), Degradation of Natural Building Stone, Geotechnical Special Publication No. 72, ASCE, Reston, pp. 85–104.

Bradley, F., 2001. Fine Marble in Architecture. WW Norton, New York.

Cardani, D., Meda, A., 1999. Flexural strength and notch sensitivity in natural building stones: Carrara and Dionysos marble. Construction and Building Materials 13 (7), 393–403.

Carslaw, H.S., Jaeger, J.C., 1959. Conduction of Heat in Solids, second ed. Oxford University Press, Oxford.

Chacon, M.A., 1999. Architectural Stone: Fabrication, Installation, and Selection. Wiley, New York.
Charles, R.J., 1958. Static fatigue of glass. Journal of Applied Physics 29, 1549–1560.
Chau, K.T., Wei, X.X., 2001. Stress concentration reduction at a reinforced hole loaded by a bonded circular inclusion. Journal of Applied Mechanics ASME 68 (3), 405–411.
Chew, M.Y.L., Wong, C.W., Kang, L.H., 1998. Building Façade: A Guide to Common Defects in Tropical Climates. World Scientific, Singapore.
Cohen, J.M., Monteiro, P.J.M., 1991. Durability and integrity of marble cladding: a state-of-the-art review. ASCE, Journal of Performance and Constructed Facilities 5 (2), 113–124.
Ferrero, A.M., Marini, P., 2001. Experimental studies on the mechanical behaviour of two thermal cracked marbles. Rock Mechanics and Rock Engineering 34 (1), 57–66.
Franzini, M., 1995. Stones in monuments—natural and anthropogenic deterioration of marble artefacts. European Journal of Mineral 7 (4), 735–743.
Gauri, K.L., Bandyopadhyay, J.K., 1999. Carbonate Stone: Chemical Behavior, Durability, and Conservation. Wiley, New York.
Hertzberg, R.W., 1996. Deformation and Fracture Mechanics of Engineering Materials, fourth ed. Wiley, New York.
Ho, K.C., Chau, K.T., 1997. An infinite plane loaded by a rivet of a different material. International Journal of Solids and Structures 34 (19), 2477–2496.
Ho, K.C., Chau, K.T., 1999. A finite strip loaded by a bonded-rivet of a different material. Computers and Structures 70 (2), 203–218.
Hook, G., 1994. Look out below—the Amoco buildings cladding failure: what went wrong, how it was fixed and the implications for thin-stone veneers. Progressive Architecture 75 (2), 58–61.
Jaeger, J.C., Cook, N.G.W., 1976. Fundamentals of Rock Mechanics, second ed. Halsted Press, New York.
Kent, C., 1990. Skin graft for Amoco building. Progressive Architecture 71 (10), 23.
Leiss, B., Weiss, T., 2000. Fabric anisotropy and its influence on physical weathering of different types of Carrara marbles. Journal of Structural Geology 22 (11–12), 1737–1745.
Lewis, M.D., 1995. Modern Stone Cladding: Design and Installation of Exterior Dimension Stone Systems, ASTM Manual Series: MNL 21, ASTM Philadelphia.
Logan, J.M., Hastedt, M., Lehnert, D., Denton, M., 1993. A case study of the properties of marble as building veneer. International Journal of Rock Mechanics and Mining Science and Geomechanics Abstracts 30 (7), 1531–1537.
Mahmutoglu, Y., 1998. Mechanical behaviour of cyclically heated fine grained rock. Rock Mechanics and Rock Engineering 31 (3), 169–179.
Miura, K., Okui, Y., Horii, H., 2003. Micromechanics-based prediction of creep failure of hard rock for long-term safety of high-level radioactive waste disposal system. Mechanics of Materials 35 (3-6), 587–601.
Press, W.H., Flannery, B.P., Teukolsky, S.A., Vetterling, W.T., 1992. Numerical Recipes: The Art of Scientific Computing, second ed. Cambridge University Press, New York.
Quick, G.W., 1998. CSIRO Methods for Testing Stone Tiles, CSIRO BCE Doc. 98/016.
Rayleigh, L., 1934. The bending of marble. Proceedings of the Royal Society of London. Series A 144 (852), 266–279.
Ridout, G., 1989. Losing its marble, Building, April 28, 1989, 17, 61.
Rizk, A.E.A., 1994. Edge-cracked plate with one free and one constrained boundary subjected to sudden convective cooling. Journal of Thermal Stresses 17 (3), 453–469.
Rizk, A.E.A., Radwan, S.F., 1992. Transient thermal-stress problem for a cracked semi-infinite medium. Journal of Thermal Stresses 15 (4), 451–468.
Rizk, A.E.A., Radwan, S.F., 1993. Fracture of a plate under transient thermal-stresses. Journal of Thermal Stresses 16 (1), 79–102.
Rooke, D.P., Cartwright, D.J., 1976. Compendium of Stress Intensity Factors. Her Majesty's Stationery Office, London.
Royer-Carfagni, G., 1999a. Some considerations on the warping of marble facades: the example of Alvar Aalto's Finland Hall in Helsinki. Construction and Building Materials 13 (8), 449–457.
Royer-Carfagni, G., 1999b. On the thermal degradation of marble. International Journal of Rock Mechanics and Mining Sciences 36 (1), 119–126.
Royer-Carfagni, C., Salvatore, W., 2000. The characterization of marble by cyclic compression loading: experimental results. Mechanics of Cohesive and Frictional Materials 5 (7), 535–563.
Rudnicki, J.W., 2000. Geomechanics. International Journal of Solids and Structures 37 (1–2), 349–358.
Ruggiero, S., 1995. Cladding's ticking time bombs. Progressive Architecture 76 (12), 90–94.
Sglavo, V.M., Bosetti, P., Trentini, E., Ceschini, M., 1999. Sandwiched-beam procedure for precracking brittle materials. Journal of American Ceramic Society 82 (8), 2269–2272.
Siegesmund, S., Ullemeyer, K., Weiss, T., Tschegg, E.K., 2000. Physical weathering of marbles caused by anisotropic thermal expansion. International Journal of Earth Sciences 89 (1), 170–182.
Simmons, G., Richter, D., 1993. Cracks in building stone. International Journal of Rock Mechanics and Mining Science and Geomechanics Abstracts 30 (7), 1553–1557.

Smith, M.R., 1999. Stone: Building Stone, Rock Fill and Armourstone in Construction, Geological Society Engineering Geology Special Publication No. 16, The Geological Society, London.

Tada, H., Paris, P.C., Irwin, G.R., 1985. The Stress Analysis of Crack Handbook, Del Research Corporation, St. Louis.

Trewhitt, J., Tuchmann, J., 1988. Amoco may replace marble on Chicago headquarters, Engineering News Record, March 24, pp. 11–12.

Widhalm, C., Tschegg, E., Eppensteiner, W., 1996. Anisotropic thermal expansion causes deformation of marble claddings. ASCE Journal of Performance of Constructed Facilities 10 (1), 5–10.

Winkler, E.M., 1975. Stone: Properties, Durability in Man's Environment, second ed. Springer, Wien.

Winkler, E.M., 1994. Stone in Architecture, third ed. Springer, Berlin.

Wong, R.H.C., Chau, K.T., Wang, P., 1995. Microcracking in coarse and fine grain marbles. In: Rock Mechanics, Proceedings of the 35th US Symposium, University of Nevada, Reno, Lake Tahoe, USA, June 5–7, 1995, pp. 477–482.

Wong, R.H.C., Chau, K.T., Wang, P., 1996. Microcracking and grain size effect in Yuen Long marbles. International Journal of Rock Mechanics and Mining Science and Geomechanics Abstract 33 (5), 479–485.